ARL-TR-8889 ● JAN 2020

Theoretical Underpinnings of Spin-Balance Machines for Measuring Mass Imbalance of Projectiles and Determining Its Effect on the Trajectory Deflection

by Paul Weinacht, Tom Puckett, James Garner, and Greg Oberlin

NOTICES

Disclaimers

The findings in this report are not to be construed as an official Department of the Army position unless so designated by other authorized documents.

Citation of manufacturer's or trade names does not constitute an official endorsement or approval of the use thereof.

Destroy this report when it is no longer needed. Do not return it to the originator.

ARL-TR-8889 ● JAN 2020

Theoretical Underpinnings of Spin-Balance Machines for Measuring Mass Imbalance of Projectiles and Determining Its Effect on the Trajectory Deflection

Paul Weinacht, Tom Puckett, James Garner, and Greg Oberlin
Weapons and Materials Research Directorate, CCDC Army Research Laboratory

REPORT DOCUMENTATION PAGE

Form Approved
OMB No. 0704-0188

1. REPORT DATE *(DD-MM-YYYY)*	2. REPORT TYPE	3. DATES COVERED (From - To)
January 2020	Technical Report	June 2017–December 2019

4. TITLE AND SUBTITLE
Theoretical Underpinnings of Spin-Balance Machines for Measuring Mass Imbalance of Projectiles and Determining Its Effect on the Trajectory Deflection

5a. CONTRACT NUMBER

5b. GRANT NUMBER

5c. PROGRAM ELEMENT NUMBER

6. AUTHOR(S)
Paul Weinacht, Tom Puckett, James Garner, and Greg Oberlin

5d. PROJECT NUMBER

5e. TASK NUMBER

5f. WORK UNIT NUMBER

7. PERFORMING ORGANIZATION NAME(S) AND ADDRESS(ES)
CCDC Army Research Laboratory
ATTN: FCDD-RLW-LE
Aberdeen Proving Ground, MD 21005

8. PERFORMING ORGANIZATION REPORT NUMBER
ARL-TR-8889

9. SPONSORING/MONITORING AGENCY NAME(S) AND ADDRESS(ES)

10. SPONSOR/MONITOR'S ACRONYM(S)

11. SPONSOR/MONITOR'S REPORT NUMBER(S)

12. DISTRIBUTION/AVAILABILITY STATEMENT
Approved for public release; distribution is unlimited.

13. SUPPLEMENTARY NOTES

14. ABSTRACT
Spin balancing is used to determine the mass imbalance of rotating machinery parts. Recently, the US Army Combat Capabilities Development Command Army Research Laboratory commissioned the development and construction of a spin-balance machine for measuring the mass imbalance of projectiles. Mass imbalance is one source of error that contributes to increased target impact dispersion and reduced hit probability. Such a machine would be useful in assessing and quantifying the mass imbalance of as-manufactured projectiles or recovered postlaunch projectiles. The current report presents the theory behind the operation of these machines and how they are used to measure the static and dynamic imbalance of projectiles. The report also provides analysis that links the measured static and dynamic imbalance to the trajectory deflection produced by the mass imbalance. Results of measured imbalance of a set of calibration pins are presented to benchmark the measurement capability. The methodology is also used to predict the trajectory deflection of a 20-mm projectile with a mass asymmetry, and the predictions are validated with previously published results.

15. SUBJECT TERMS
projectile mass imbalance, dispersion, trajectory deflection, spin balancing, lateral throw-off

16. SECURITY CLASSIFICATION OF:			17. LIMITATION OF ABSTRACT	18. NUMBER OF PAGES	19a. NAME OF RESPONSIBLE PERSON
a. REPORT	b. ABSTRACT	c. THIS PAGE			Paul Weinacht
Unclassified	Unclassified	Unclassified	UU	44	19b. TELEPHONE NUMBER (Include area code) (410) 306-0800

Contents

List of Figures

List of Tables

Acknowledgment

The original inspiration for the investigation and eventual procurement of the spin-balance machines by US Army Combat Capabilities Development Command Army Research Laboratory (ARL) was made by Jim Garner, Flight Sciences Branch, ARL. Subsequent application of these machines to measure the spin imbalance of projectiles led to the need to more fully understand the operation of these machines and how the measured imbalance quantities could be more directly tied to projectile trajectory deflection. This is the subject of this report.

1. Introduction

The US Army Combat Capabilities Development Command Army Research Laboratory (ARL) has been investigating small-arms accuracy with the aim of developing the scientific and technical understanding necessary to improve the accuracy of current and future ammunition and weapon systems. Accuracy is a fairly complex subject, and there are many different contributors that influence the accuracy of the ammunition and weapon system. One source of inaccuracy is the mass imbalance of the ammunition. To quantify these effects, ARL commissioned the development and construction of a spin-balance machine to quantify the mass imbalance of small-caliber ammunition. The purpose of the current work is to present some of the theoretical background on the operation of this type of machine and tie the imbalance measurements made using the machine to the ballistic parameters that more directly quantify the effect that imbalance has on the accuracy of a projectile.

The general theory and operation of the spin-balance machine is discussed in reports by the American Hofmann Corporation,[1,2] which provide some background required to operate the spin-balance machine commissioned by ARL. However, since the intended application is to assess the static and dynamic imbalance of projectiles, some additional theoretical background could be helpful in understanding how a machine of this type performs the imbalance measurements and how the measurements can be translated to the intended application. Because ARL's spin-balance machine is a commercial product, there are aspects of its operation that have to be treated as "black-box", but it seems reasonable that theoretical aspects of its operation can be deduced and a better understanding of the measured data can be obtained.

This report presents the theoretical background as well as representative results obtained using the spin-balance machine. Section 2 of this report presents the spin-balance machine setup. Section 3 presents some of the theoretical background that relates the effect of an arbitrary number of mass asymmetries as either mass imbalances at two "correction" planes or as an equivalent static and couple imbalance. While the mass imbalance of a projectile is useful information, how the measured imbalance is connected to the trajectory deflection is ultimately the result of primary interest. This analysis is presented in Section 4. Section 5 presents results for a 20-mm projectile with a mass imbalance. Using the known imbalance, results are obtained for hypothetically derived spin-balance measurements, which are then used to determine the predicted mass imbalance from the spin-balance machine and the subsequent trajectory deflection. The results are compared with existing theoretical predictions and experimental measurements. Finally,

measurements of the spin imbalance of a set of calibration pins are presented in Section 6 to further benchmark the measurement capability.

2. Spin-Balance Machine Setup

Figures 1 and 2 show photographs of the spin-balance machine commissioned by ARL.

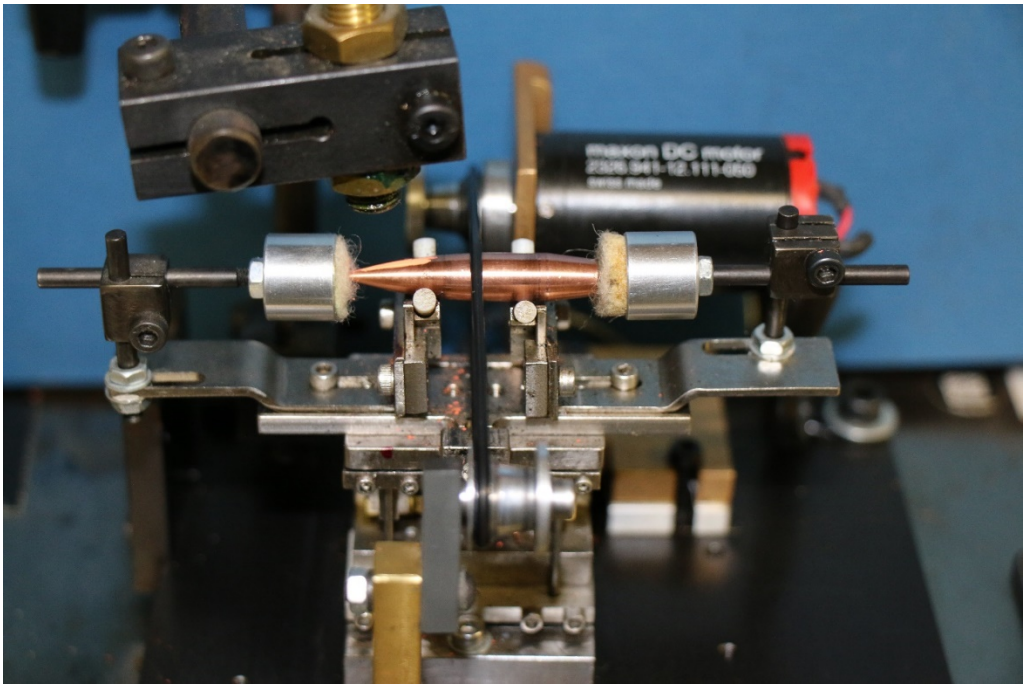

Fig. 1 ARL spin-balance machine

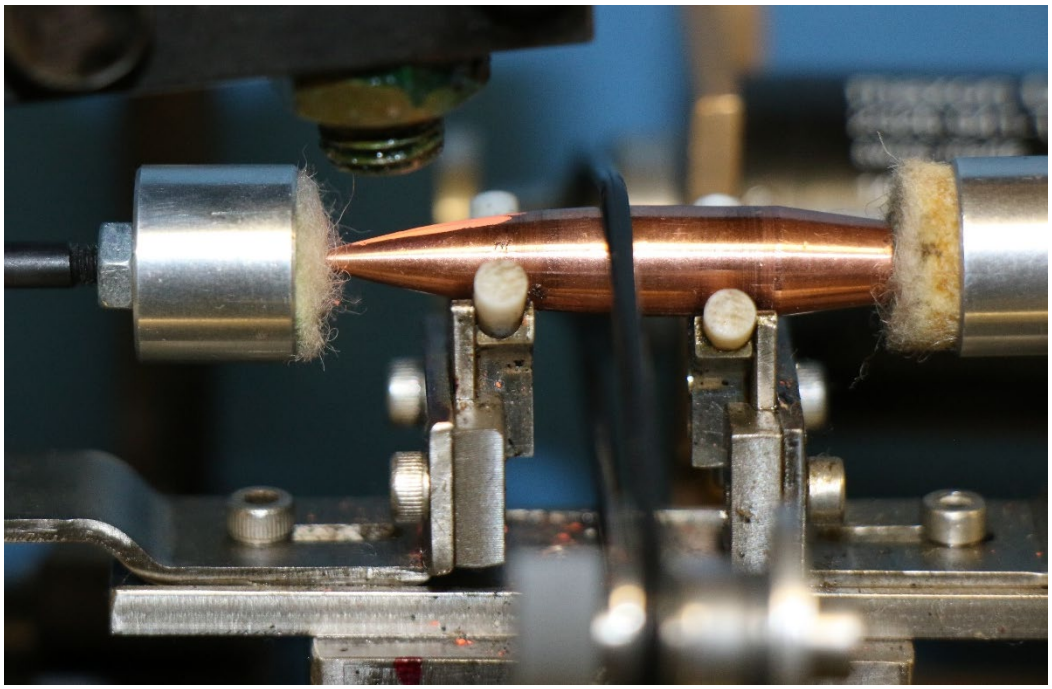

Fig. 2 Close-up of ARL spin-balance machine

Figure 3 shows a planform view of the spin-balancing setup. There is a reference mark on the spin-balance machine from which lengths along the axial direction of the part are measured. The spin-measurement machine uses the required length measurements relative to the reference mark as part of its internal calculations. For certain applications (in particular, if the imbalance is to be corrected with the part in the spin-balance machine), the location of the pickup locations and the corrections planes relative to the reference mark are sufficient to define all the necessary lengths for the operation of the spin-balance machine. However, if the location of the measured imbalances are required to be known relative to the measured part itself (particularly once the part is to be removed from the spin-balance machine), an additional reference point associated with the part itself must be established relative to the reference mark on the spin-balance machine itself. For example, if the measured imbalances are to be used to determine the lateral throw-off of a projectile in flight, the location of the imbalances on the projectile would be determined from the distance of the reference mark on the spin-balance machine relative to the nose of the projectile, L_{ref}.

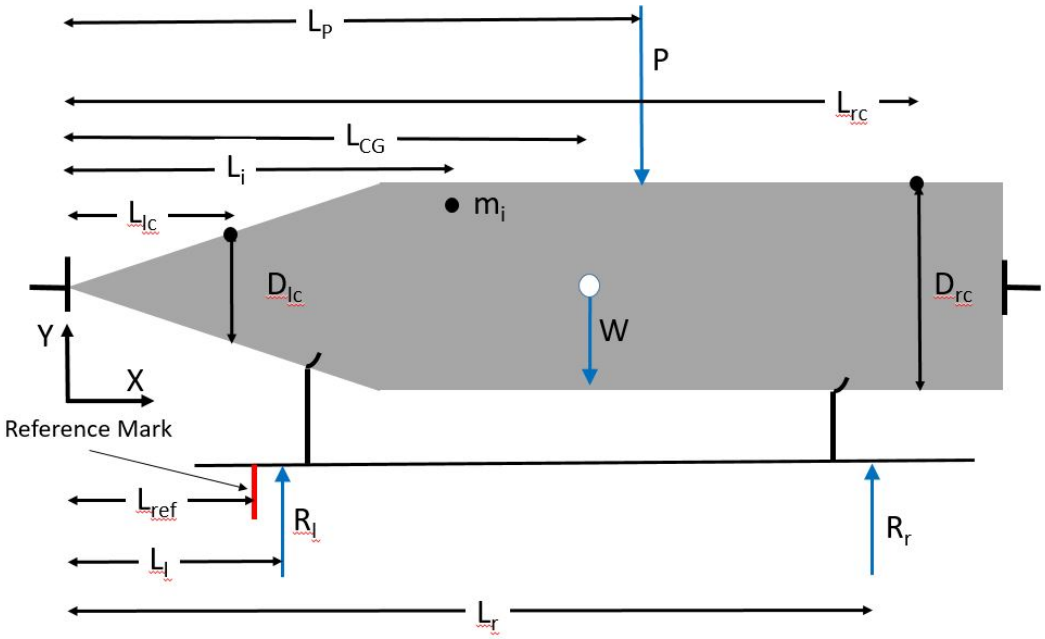

Fig. 3 Planform view of spin-balance machine setup (facing front of spin-balancing machine)

The part being measured rides on two V-blocks that are adjusted so that the part rides smoothly. The precise location of the V-blocks is not measured in the spin-balance procedure and does not directly enter into the measurement calculations. There does not appear to be a requirement that the cylindrical portion of the projectile ride on the V-blocks. In other words, the projectile could ride on the forward ogive and/or the aft boattail. A belt is used to rotate the part in the V-blocks. The belt provides a constant downward force P at a location L_P on the measured part. The weight of the part W acts at the center of gravity of the part L_{CG}. The belt force and part weight and their location appear in the analysis discussed below, but do not directly play into the measurement of the imbalance to the extent that these are quantities would need to be explicitly specified for the spin-balance machine measurements.

The spin-balance machine measures the forces R_l and R_r at the two pickup locations L_l and L_r. Based on the measured forces from the pickups, the spin-balance machine computes the imbalance. In many applications, the spin-balance machine would be used to correct the imbalance on the part. This can be done by adding or removing mass from the part at two locations (correction planes) along the length of the part shown as L_{lc} and L_{rc} in Fig. 3. Since the correction is typically made at the surface of the part, the diameter of the part at the correction plane D_{lc} and D_{rc} is also specified. The corrections at each correction plane are also made at specified circumferential locations $\emptyset_{lc}$ and $\emptyset_{rc}$, as shown in Fig. 4. The correction planes are suitable locations selected for the imbalance to be

corrected without interfering with the operation of the part. For example, for projectile applications the cylindrical portion of the projectile may be a poor location for the correction to be made because this portion of the projectile contacts the gun barrel during the firing process, and any correction may be eliminated by the engraving process during firing. If the purpose of the imbalance measurement was simply to define the degree of imbalance, the selection of the location of the correction planes as well as the diameter at the correction plane are somewhat arbitrary.

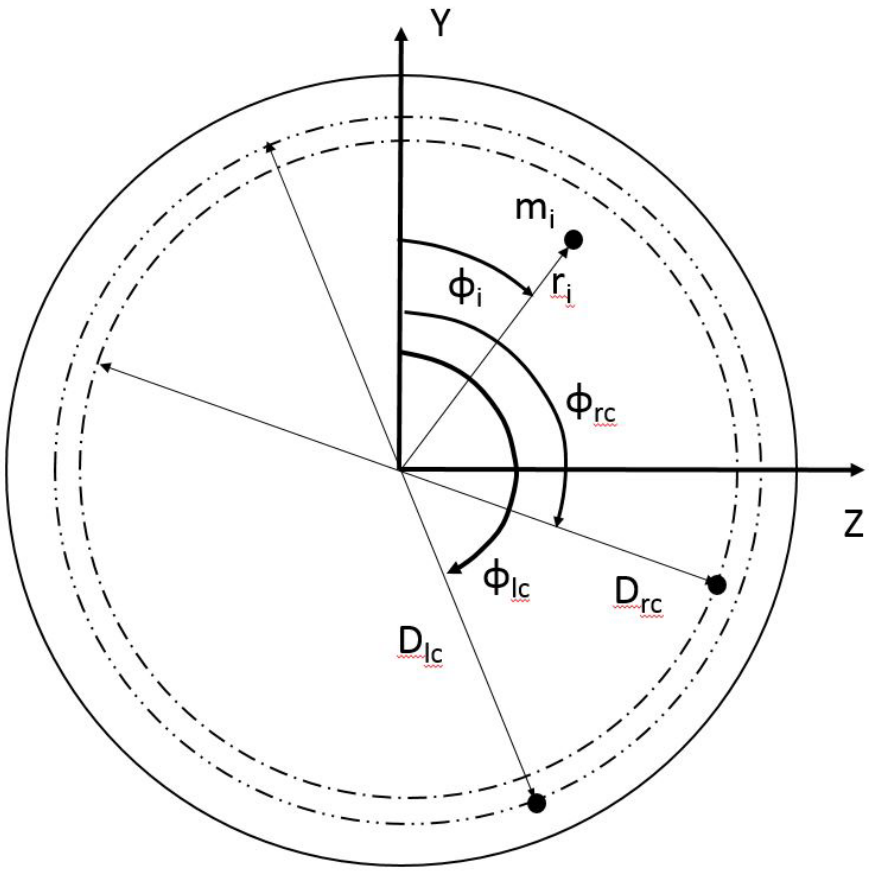

Fig. 4 Cross-sectional view of spin-balance machine setup viewed from left side of fixture

Figure 3 shows the part being measured with the nose to the left when viewed from the front of the machine. The fixture is capable of measuring parts and correcting imbalances with the nose oriented to either the left or right. However, if the part is measured with the nose right, care must be taken in analyzing the resulting measurements, particularly if they are used to quantify the ballistic performance, since the analysis presented here assumes that the nose is oriented to the left. At a minimum, the measured angular orientations $\emptyset_{lc}$ and $\emptyset_{rc}$ will likely have to be reversed in sign.

3. Theoretical Background of the Spin-Balance Machine Operation

As indicated previously, the spin-balance machine measures the imbalance of a rotating part by measuring the forces at two pickup locations. The part may have an arbitrary number of mass asymmetries that contribute to the overall imbalance of the part. To be useful for quantifying the effect of the imbalance on the ballistic performance of the projectile, the static and couple imbalance of the part needs to be determined from the measured pickup forces. As well, the mass imbalance from an arbitrary number of mass asymmetries can be shown to produce the same static and couple imbalance as imbalances at two correction planes that, if corrected, will produce a balanced part with no static or couple (dynamic) imbalance. By relating 1) the imbalance due to an arbitrary number of mass asymmetries to the measured pickup forces (Section 3.1), 2) the mass imbalance at two correction planes to the measured pickup forces (Section 3.2), and 3) static and couple imbalance to the measured pickup forces (Section 3.3), the interrelation of all three types of imbalance can be determined. Essentially, the analysis shows that an arbitrary number of mass imbalances within the part can be represented by a static and couple imbalance, and that the imbalance can be eliminated by appropriate corrections at two locations on the projectile. The current spin-balance system outputs the imbalance in terms of the mass imbalance at two correction planes. While the current system also outputs a static and couple imbalance, it is advisable to use the mass imbalance at the two correction planes to calculate the static and couple imbalance using the equations presented in the following, as discussed in Section 3.4.

3.1 Equations of Motion of Arbitrary Mass Asymmetries

A given part may have an arbitrary number of mass asymmetries located at various locations throughout the part. Although it may be difficult to determine the exact magnitude and location of each asymmetry, the analysis here provides the first step in representing the net effect of an arbitrary number of asymmetries within the part. A summation of the forces in the vertical direction and the moments acting normal to the vertical plane at a point L_1 along the centerline of the part is shown in Eqs. 1 and 2.

$$\sum F_Y = R_l + R_r - P - W + \sum_{i=1}^{i=N} F_i \cos(\emptyset_i + \emptyset) = 0 \qquad (1)$$

$$\sum M_Z|_{L_l} = -P(L_P - L_l) - W(L_{CG} - L_l) + R_r(L_r - L_l) + \sum_{i=1}^{i=N} F_i(L_i - L_l)\cos(\emptyset_i + \emptyset) = 0 \quad (2)$$

F_i is the centrifugal force due the individual mass asymmetry, ω is the rotation speed of the part, m_i is the mass of each individual asymmetry and r_i is the radial location of the asymmetry from the axis of rotation, $\emptyset_i$ is the circumferential location of the asymmetry from the vertical axis, and $\emptyset$ is the circumferential location of the part from the vertical axis as it rotates about its longitudinal axis. The mass asymmetry is considered a positive mass, but voids in a part could be considered as negative mass. U_i is the imbalance due to the individual mass asymmetry.

$$F_s = \omega^2 U_s = \omega^2 m_s r_s \quad (3)$$

Using Eqs. 1 and 2, the pickup forces R_l and R_r can be determined.

$$R_r = P\frac{(L_P - L_l)}{(L_r - L_l)} + W\frac{(L_{CG} - L_l)}{(L_r - L_l)} - \sum_{i=1}^{i=N} F_i\frac{(L_i - L_l)}{(L_r - L_l)}\cos(\emptyset_i + \emptyset) \quad (4)$$

$$R_l = P\left[1 - \frac{(L_i - L_l)}{(L_r - L_l)}\right] + W\left[1 - \frac{(L_{CG} - L_l)}{(L_r - L_1)}\right] - \sum_{i=1}^{i=N} F_i\left[1 - \frac{(L_i - L_l)}{(L_r - L_l)}\right]\cos(\emptyset_i + \emptyset) \quad (5)$$

As shown in Eqs. 4 and 5, the pickup forces consist of a constant average component due to the belt tension and the projectile weight, and a fluctuating component due to the mass asymmetries that varies periodically as the projectile rotates during the spin balancing. As shown in Eqs. 6–13, the net response on each pickup due to an arbitrary number of mass asymmetries can be represented as a single sinusoidal response with an appropriate phase offset. By measuring the amplitude and phase angle of the fluctuating components of the reaction forces, the net effect of the mass asymmetries can be determined.

$$R_r = P\frac{(L_P - L_l)}{(L_r - L_l)} + W\frac{(L_{CG} - L_l)}{(L_r - L_l)} + \tilde{R}_r\cos(\tilde{\emptyset}_r + \emptyset) \quad (6)$$

$$R_l = P\left[1 - \frac{(L_P - L_l)}{(L_r - L_l)}\right] + W\left[1 - \frac{(L_{CG} - L_l)}{(L_r - L_1)}\right] + \tilde{R}_l\cos(\tilde{\emptyset}_l + \emptyset) \quad (7)$$

where

$$\tilde{R}_r\cos(\tilde{\emptyset}_r) = -\sum_{i=1}^{i=N} F_i\cos(\emptyset_i)\frac{(L_i - L_l)}{(L_r - L_l)} \quad (8)$$

$$\tilde{R}_r \sin\left(\widetilde{\emptyset}_r\right) = -\sum_{i=1}^{i=N} F_i \sin(\emptyset_i) \frac{(L_i - L_l)}{(L_r - L_l)} \tag{9}$$

$$\tilde{R}_r = \sqrt{\left(\sum_{i=1}^{i=N} F_i \cos(\emptyset_i) \frac{(L_i - L_l)}{(L_r - L_l)}\right)^2 + \left(\sum_{i=1}^{i=N} F_i \sin(\emptyset_i) \frac{(L_i - L_l)}{(L_r - L_l)}\right)^2} \tag{10}$$

$$\tilde{R}_l \cos\left(\widetilde{\emptyset}_l\right) = -\sum_{i=1}^{i=N} F_i \cos(\emptyset_i) \left[1 - \frac{(L_i - L_l)}{(L_r - L_l)}\right] \tag{11}$$

$$\tilde{R}_l \sin\left(\widetilde{\emptyset}_l\right) = -\sum_{i=1}^{i=N} F_i \sin(\emptyset_i) \left[1 - \frac{(L_i - L_l)}{(L_r - L_l)}\right] \tag{12}$$

$$\tilde{R}_l = \sqrt{\left(\sum_{i=1}^{i=N} F_i \cos(\emptyset_i) \left[1 - \frac{(L_i - L_l)}{(L_r - L_l)}\right]\right)^2 + \left(\sum_{i=1}^{i=N} F_i \sin(\emptyset_i) \left[1 - \frac{(L_i - L_l)}{(L_r - L_l)}\right]\right)^2} \tag{13}$$

The phase angles of the imbalance $\widetilde{\emptyset_r}$ and $\widetilde{\emptyset_l}$ are determined from the appropriate application of the arctangent function using Eqs. 8 and 9 or Eqs. 11 and 12, respectively.

The pickup forces for a hypothetical mass offset case that contains four individual mass asymmetries (parameter listed in Table 1) are shown in Fig. 5. As shown in the previous analysis, there is a mean contribution from the belt tension and part weight and a fluctuating component from the mass asymmetries that is sinusoidal in nature. The amplitude of the fluctuating component of the pickup forces varies with the square of the rotation rate of the spin-balance machine. As a result, sufficient spin rate must be applied for a measurable fluctuating component to be accurately measured.

Table 1 Sample parameters for spin-balance measurement

Belt force, P (N)	0.5			
Belt axial location, L_P (cm)	1.39			
Part weight, W (g)	4.0			
Part center of gravity location, L_{CG} (cm)	1.529			
Rotation rate (rad/s)	150			
Left pickup location (cm)	0.278			
Right pickup location (cm)	2.502			
Imbalance	i = 1	i = 2	i = 3	i = 4
Imbalance axial location, L_i (cm)	1.112	1.946	1.112	1.668
Imbalance radial location, r_i (cm)	0.278	0.278	0.278	0.278
Imbalance mass, m_i (g)	0.04	0.04	0.04	0.04
Imbalance circumferential location φ_i (deg)	45.0	135.0	25.0	225.0

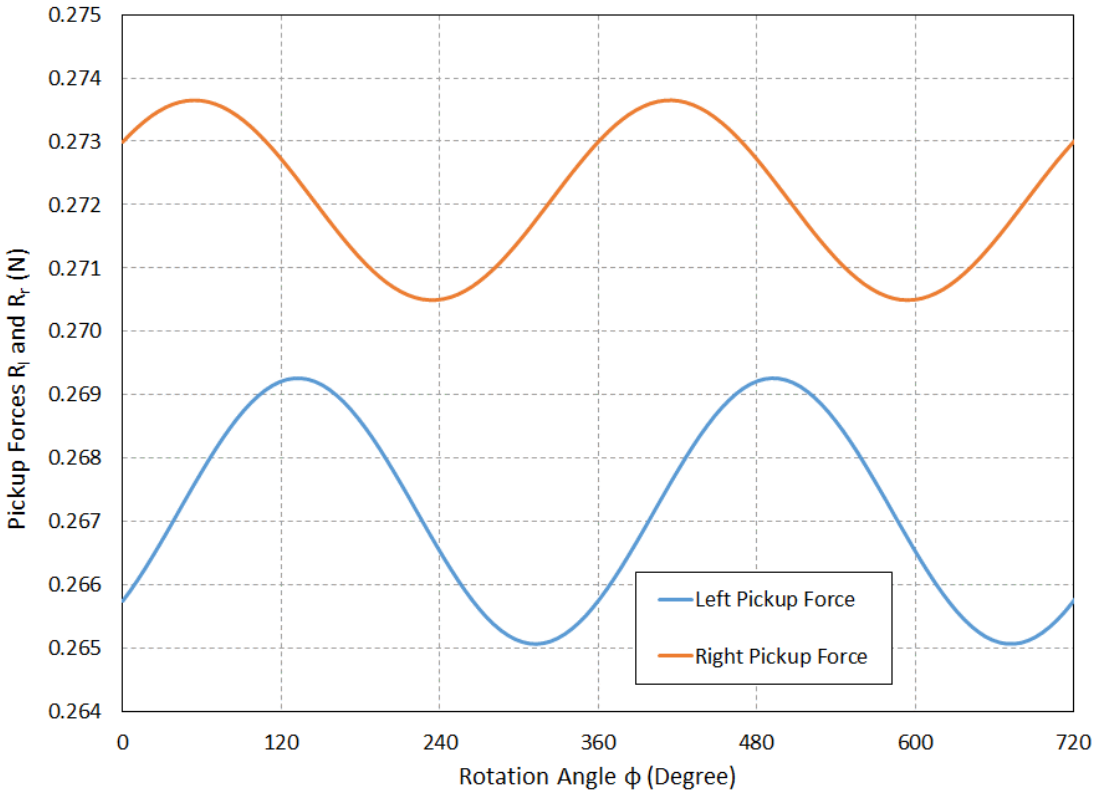

Fig. 5 Pickup forces on left and right pickups

3.2 Equations of Motion of Mass Offsets at Two Correction Planes

The spin-balance machine characterizes the effect of an arbitrary number of mass asymmetries as mass imbalances located at the two correction planes. The force and moment equations for effective mass imbalances at the two correction planes are shown in Eqs. 14 and 15. This set of equations can be related to the equations in Section 3.1 to obtain the relationship between an arbitrary number of mass asymmetries and an equivalent representation as two mass offsets at the two correction planes.

$$\sum F_Y = R_l + R_r - P - W + F_{lc}\cos(\emptyset_{lc} + \emptyset) + F_{rc}\cos(\emptyset_{rc} + \emptyset) = 0 \tag{14}$$

$$\begin{aligned}\sum M_Z|_{L_l} = -P(L_P - L_l) - W(L_{CG} - L_l) + R_r(L_r - L_l) + F_{lc}(L_{lc} - L_l)\cos(\emptyset_{lc} + \emptyset) \\ +F_{rc}(L_{rc} - L_l)\cos(\emptyset_{rc} + \emptyset) = 0\end{aligned} \tag{15}$$

Here, F_{lc} and F_{rc} are the forces due to the mass imbalance at the left and right correction planes; m_{lc} and m_{rc} are the equivalent masses of the imbalance at the left and right correction planes; L_{lc} and L_{rc} are the axial locations of the left and right correction planes; and r_{lc} and r_{rc} and $\emptyset_{lc}$ and $\emptyset_{rc}$ are the radial and circumferential locations, respectively, of the imbalance at the left and right correction planes. The axial location and radial distance (actually input as a diameter) at both correction planes are required to be input into the spin-balance machine software. If the spin-balance machine is to be used to measure the imbalance and no correction is to be made to the part, the selection of the axial location and radial distance of the correction at both correction planes is somewhat arbitrary:

$$F_{lc} = \omega^2 m_{lc} r_{lc} = \omega^2 U_{lc} \tag{16}$$

$$F_{rc} = \omega^2 m_{rc} r_{rc} = \omega^2 U_{rc} \tag{17}$$

The pickup forces due to mass imbalance at the two corrections planes is shown in the following equations:

$$\begin{aligned}R_r = P\frac{(L_P - L_l)}{(L_r - L_l)} + W\frac{(L_{CG} - L_l)}{(L_r - L_l)} - F_{lc}\frac{(L_{lc} - L_l)}{(L_r - L_l)}\cos(\emptyset_{lc} + \emptyset) \\ - F_{rc}\frac{(L_{rc} - L_l)}{(L_r - L_l)}\cos(\emptyset_{rc} + \emptyset)\end{aligned} \tag{18}$$

$$R_l = P\left[1 - \frac{(L_P - L_l)}{(L_r - L_l)}\right] + W\left[1 - \frac{(L_{CG} - L_l)}{(L_r - L_l)}\right] - F_{lc}\left[1 - \frac{(L_{lc} - L_l)}{(L_r - L_l)}\right]\cos(\emptyset_{lc} + \emptyset) - F_{rc}\left[1 - \frac{(L_{rc} - L_l)}{(L_r - L_l)}\right]\cos(\emptyset_{rc} + \emptyset) \quad (19)$$

The equivalent mass imbalance at the two correction planes can be related to the arbitrary mass imbalance, as shown in Eqs. 20–25:

$$F_{lc}\cos(\emptyset_{lc}) = -\sum_{i=1}^{i=N} F_i\cos(\emptyset_i)\frac{(L_i - L_{rc})}{(L_{rc} - L_{lc})} \quad (20)$$

$$F_{lc}\sin(\emptyset_{lc}) = -\sum_{i=1}^{i=N} F_i\sin(\emptyset_i)\frac{(L_i - L_{rc})}{(L_{rc} - L_{lc})} \quad (21)$$

$$F_{rc}\cos(\emptyset_{rc}) = \sum_{i=1}^{i=N} F_i\cos(\emptyset_i)\frac{(L_i - L_{lc})}{(L_{rc} - L_{lc})} \quad (22)$$

$$F_{rc}\sin(\emptyset_{rc}) = \sum_{i=1}^{i=N} F_i\sin(\emptyset_i)\frac{(L_i - L_{lc})}{(L_{rc} - L_{lc})} \quad (23)$$

$$F_{lc} = \sqrt{\left(\sum_{i=1}^{i=N} F_i\cos(\emptyset_i)\frac{(L_i - L_{rc})}{(L_{rc} - L_{lc})}\right)^2 + \left(\sum_{i=1}^{i=N} F_i\sin(\emptyset_i)\frac{(L_i - L_{rc})}{(L_{rc} - L_{lc})}\right)^2} \quad (24)$$

$$F_{rc} = \sqrt{\left(\sum_{i=1}^{i=N} F_i\cos(\emptyset_i)\frac{(L_i - L_{lc})}{(L_{rc} - L_{lc})}\right)^2 + \left(\sum_{i=1}^{i=N} F_i\sin(\emptyset_i)\frac{(L_i - L_{lc})}{(L_{rc} - L_{lc})}\right)^2} \quad (25)$$

The phase angles of the imbalance $\emptyset_{lc}$ and $\emptyset_{rc}$ are determined from the appropriate application of the arctangent function using Eqs. 20 and 21 or Eqs. 22 and 23, respectively.

As shown in Eqs. 6 and 7, the pickup forces contain a constant force due to the force from the belt *P* and the weight of the part *W*. There is also a fluctuating component of the pickup forces (Eqs. 6 and 7). As shown in Eqs. 26–29, the amplitude of the pickup forces $\tilde{R}_l$ and $\tilde{R}_r$ and associated phase angles $\widetilde{\emptyset}_r$ and $\widetilde{\emptyset}_L$ can be used to determine the mass imbalance F_{lc} and F_{rc} and associated phase angles, which serve as one of the primary measures of the imbalance of the part and are the basis of establishing the mass correction required to balance the part. Presumably, these calculations are done internally within the spin-balance machine. If the two correction planes are located at the same location as the two pickup

locations, as expected the pickup forces $\tilde{R}_l$ and $\tilde{R}_r$ are opposite in sign to the forces due to the mass imbalance F_{lc} and F_{rc}.

$$F_{lc}\cos(\emptyset_{lc}) = \tilde{R}_r \frac{(L_r - L_{rc})}{(L_{rc} - L_{lc})}\cos(\widetilde{\emptyset}_r) + \tilde{R}_l \frac{(L_l - L_{rc})}{(L_{rc} - L_{lc})}\cos(\widetilde{\emptyset}_l) \tag{26}$$

$$F_{lc}\sin(\emptyset_{lc}) = \tilde{R}_r \frac{(L_r - L_{rc})}{(L_{rc} - L_{lc})}\sin(\widetilde{\emptyset}_r) + \tilde{R}_l \frac{(L_l - L_{rc})}{(L_{rc} - L_{lc})}\sin(\widetilde{\emptyset}_l) \tag{27}$$

$$F_{rc}\cos(\emptyset_{rc}) = -\tilde{R}_r \frac{(L_r - L_{lc})}{(L_{rc} - L_{lc})}\cos(\widetilde{\emptyset}_r) - \tilde{R}_l \frac{(L_l - L_{lc})}{(L_{rc} - L_{lc})}\cos(\widetilde{\emptyset}_l) \tag{28}$$

$$F_{rc}\sin(\emptyset_{rc}) = -\tilde{R}_r \frac{(L_r - L_{lc})}{(L_{rc} - L_{lc})}\sin(\widetilde{\emptyset}_r) - \tilde{R}_l \frac{(L_l - L_{lc})}{(L_{rc} - L_{lc})}\sin(\widetilde{\emptyset}_l) \tag{29}$$

As before, the magnitude of the imbalance forces F_{lc} and F_{rc} is determined from the root sum squares of Eqs. 26 and 27 and Eqs. 28 and 29, respectively, while the phase angles of the imbalance $\emptyset_{lc}$ and $\emptyset_{rc}$ are determined from the appropriate application of the arctangent function using Eqs. 26 and 27 or Eqs. 28 and 29, respectively.

The analysis in this section presents the equivalent representation of the mass imbalance of a part due to an arbitrary number of mass imbalances using individual mass imbalances located two correction planes. Note that the imbalances presented here represent the actual mass imbalance of the part, not the correction required to balance the part. In the analysis here, the mass imbalances are considered positive for mass addition and negative for mass removal (or mass void). The imbalance of the part is characterized in terms of the imbalance masses, m_{lc} and m_{rc} at the left and right correction planes, the imbalance phase angles $\emptyset_{lc}$ and $\emptyset_{rc}$, and the axial and radial location of the corrections, L_{lc} and L_{rc} and r_{lc} and r_{rc}. The imbalance U_{lc} and U_{rc} and imbalance mass m_{lc} and m_{rc} are determined from Eqs. 16 and 17 using the imbalance forces F_{lc} and F_{rc} determined from the pickup forces.

The spin-balance machine typically outputs the mass correction rather than the actual mass imbalance. There are two modes for the correction for the spin-balance machine, either mass addition or mass removal. To characterize the mass imbalance properly, if spin-balance machine is used in mass addition mode, the output spin-balance corrections correspond to a negative mass imbalance at the same locations or a positive mass imbalance located at 180° to the imbalance phase angles $\emptyset_{lc}$ and $\emptyset_{rc}$.

3.3 Equations of Motion of Dynamic Imbalance due to a Static and Couple Imbalance

An arbitrary number of mass asymmetries produces a dynamic imbalance can be more universally characterized by a static imbalance produced by the displacement of the center of gravity of the part from the axis of rotation and a couple imbalance that contributes to the dynamic imbalance of the part. The static imbalance can be represented as a single mass offset from the axis of rotation and can be positioned at any point along the length of the part. However, for the intended ballistic application, the static imbalance is considered as the displacement of the center of gravity from the axis of rotation. For this application, it makes sense to position the static imbalance at the same longitudinal location as the center of gravity. The resulting couple is a function of the location where the static imbalance is applied. Summations of the forces and moments for this case are shown in Eqs. 30 and 31:

$$\sum F_Y = R_r + R_l - P - W + F_s\cos(\emptyset_S + \emptyset) = 0 \tag{30}$$

$$\sum M_Z|_{L_l} = -P(L_P - L_l) - W(L_{CG} - L_l) + R_r(L_r - L_l) + F_s(L_{CG} - L_l)\cos(\emptyset_S + \emptyset) + M_C\sin(\emptyset_c + \emptyset) = 0 \tag{31}$$

Here, F_S is the centrifugal force produced by the static imbalance U_S. The static imbalance U_S can be represented by a mass imbalance m_S located at a radial distance r_S from the geometric axis. The static imbalance is located at an angle $\emptyset_S$ with respect to the y-axis.

$$F_s = \omega^2 U_s = \omega^2 m_s r_s \tag{32}$$

M_C is the couple produced by the couple imbalance U_C. The vector direction of the couple imbalance is oriented at an angle phase angles $\emptyset_C$ with respect to the rotation angle of the part $\emptyset$. The couple imbalance U_C can be represented by two masses m_C separated by an axial distance L_C located at opposing circumferential locations at a radial distance r_C across the longitudinal axis (Eq. 33). Note that the vector direction of the couple is normal to the plane formed by the longitudinal axis of the part and the two masses. Other representations of the couple are possible as long as the same couple imbalance is generated. The axial location of the couple along the geometric axis is arbitrary.

$$M_C = \omega^2 U_C = \omega^2 m_C r_C L_C \tag{33}$$

The pickup forces due to mass imbalance at the static and couple imbalance is shown in Eqs. 34 and 35.

$$R_l = P\left[1 - \frac{(L_P - L_l)}{(L_r - L_l)}\right] + W\left[1 - \frac{(L_{CG} - L_l)}{(L_r - L_l)}\right] - F_S\left[1 - \frac{(L_{CG} - L_l)}{(L_r - L_l)}\right]\cos(\emptyset_S + \emptyset) + M_C\frac{1}{(L_r - L_l)}\sin(\emptyset_C + \emptyset) \quad (34)$$

$$R_r = P\frac{(L_P - L_l)}{(L_r - L_l)} + W\frac{(L_{CG} - L_l)}{(L_r - L_l)} - F_S\frac{(L_{CG} - L_l)}{(L_r - L_l)}\cos(\emptyset_S + \emptyset) - M_c\frac{1}{(L_r - L_l)}\sin(\emptyset_c + \emptyset) \quad (35)$$

Comparing Eq. 1 with Eq. 30, the force due to the static imbalance can be related to the forces due to an arbitrary number of mass asymmetries within the part:

$$F_S\cos(\emptyset_S) = \sum_{i=1}^{i=N} F_i\cos(\emptyset_i) \quad (36)$$

$$F_S\sin(\emptyset_S) = \sum_{i=1}^{i=N} F_i\sin(\emptyset_i) \quad (37)$$

Using Eqs. 36 and 37, the relation between the static imbalance and the imbalance from an arbitrary number of mass asymmetries can be obtained:

$$U_S\cos(\emptyset_S) = \sum_{i=1}^{i=N} U_i\cos(\emptyset_i) \quad (38)$$

$$U_S\sin(\emptyset_S) = \sum_{i=1}^{i=N} U_i\sin(\emptyset_i) \quad (39)$$

Similarly, by comparing Eqs. 2 and 31, the relation between the couple imbalance and the moment about the center of gravity due to an arbitrary number of mass imbalances within the part can be found:

$$M_C\cos(\emptyset_C) = -\sum_{i=1}^{i=N} F_i(L_i - L_{CG})\sin(\emptyset_i) \quad (40)$$

$$M_C\sin(\emptyset_C) = \sum_{i=1}^{i=N} F_i(L_i - L_{CG})\cos(\emptyset_i) \quad (41)$$

The couple imbalance can be obtained using Eqs. 40 and 41:

$$U_C\cos(\emptyset_C) = -\sum_{i=1}^{i=N} m_i r_i(L_i - L_{CG})\sin(\emptyset_i) \quad (42)$$

$$U_C \sin(\emptyset_C) = \sum_{i=1}^{i=N} m_i r_i (L_i - L_{CG}) \cos(\emptyset_i) \tag{43}$$

The magnitude of F_S, U_S, M_C, and U_c can be determined from the root sum squares of Eqs. 36–43, and the phase angles $\emptyset_S$ and $\emptyset_C$ are determined from the appropriate application of the arctangent function using Eqs. 36–43.

As shown in Section 3.2, the spin-balance machine captures the effect of an arbitrary number of mass imbalances as imbalances at the two correction planes. Comparing Eq. 14 with Eq. 30, the force due to the static imbalance can be related to the forces due to the imbalances at the two correction planes:

$$F_S \cos(\emptyset_S) = F_{lc} \cos(\emptyset_{lc}) + F_{rc} \cos(\emptyset_{rc}) \tag{44}$$

$$F_S sin(\emptyset_S) = F_{lc} \sin(\emptyset_{lc}) + F_{rc} \sin(\emptyset_{rc}) \tag{45}$$

or equivalently,

$$U_S \cos(\emptyset_S) = U_{lc} \cos(\emptyset_{lc}) + U_{rc} \cos(\emptyset_{rc}) \tag{46}$$

$$U_S sin(\emptyset_S) = U_{lc} \sin(\emptyset_{lc}) + U_{rc} \sin(\emptyset_{rc}) \tag{47}$$

The magnitude of the static imbalance force F_s and the static imbalance U_s is determined from the root sum squares of Eqs. 44 and 45 or Eqs. 46 and 47, respectively, and the phase angle of the static imbalance $\emptyset_s$ is determined from the appropriate application of the arctangent function using Eqs. 44 and 45 or 46 and 47. The phase angle of the static imbalance $\emptyset_s$ essentially provides the orientation of the center of gravity of the unbalanced part relative to the coordinate systems.

Similarly, comparing Eqs. 15 and 31, the couple due to the couple imbalance can be related to the forces due to the imbalance at the two correction planes:

$$M_C \cos(\emptyset_C) = -F_{lc}(L_{lc} - L_{CG}) \sin(\emptyset_{lc}) - F_{rc}(L_{rc} - L_{CG}) \sin(\emptyset_{rc}) \tag{48}$$

$$M_C \sin(\emptyset_C) = F_{lc}(L_{lc} - L_{CG}) \cos(\emptyset_{lc}) + F_{rc}(L_{rc} - L_{CG}) \cos(\emptyset_{rc}) \tag{49}$$

or equivalently,

$$U_C \cos(\emptyset_C) = -U_{lc}(L_{lc} - L_{CG}) \sin(\emptyset_{lc}) - U_{rc}(L_{rc} - L_{CG}) \sin(\emptyset_{rc}) \tag{50}$$

$$U_C \sin(\emptyset_C) = U_{lc}(L_{lc} - L_{CG}) \cos(\emptyset_{lc}) + U_{rc}(L_{rc} - L_{CG}) \cos(\emptyset_{rc}) \tag{51}$$

The magnitude of M_C and U_c can be determined from the root sum squares of Eqs. 48–51, and the phase angles $\emptyset_C$ is determined from the appropriate application of the arctangent function using Eqs. 48–51.

As stated in Section 3.2, the spin-balance machine typically outputs the mass correction rather than the actual mass imbalance. If the spin-balance machine is used in mass addition mode, the actual imbalance angles at the two correction planes used to compute the static and couple imbalance angles as shown is out of phase is 180° (π radians) with the measured correction angles from the spin-balance machine.

3.4 A Cautionary Note on the Static and Couple Imbalance as Measured by the Spin-Balance Machine

Section 3.3 provides a means of determining the static and couple imbalance from the spin-balance machine measurements of the imbalances at the two correction planes. This formulation assumes that the static imbalance is located at the center of gravity and the remaining imbalance is attributable to the couple imbalance. The resulting couple imbalance can be applied at any axial location along the part. ARL's spin-balance machine also provides a static and couple balance computation in one of the output tabulations that essentially breaks down the imbalance at the two correction planes into a static imbalance component and a couple imbalance component. Effectively, this locates the static imbalance at the midpoint between the two correction planes (which is not necessarily located at the center of gravity of the part). The remaining imbalance of the part is represented as a couple imbalance, which is a function of the location of the static imbalance. Thus, the couple imbalance from the spin-balance machine's tabulated output will not be equivalent to the couple imbalance computed using Eqs. 50 and 51 unless the center of gravity is located at the midpoint between the two correction planes. Since ballistic applications assume the static imbalance is located at the same axial location as the center of gravity, it is recommended that for ballistics applications, the mass imbalance at the two correction planes be used to directly compute the static and couple imbalance (Eqs. 46, 47, 50, and 51) rather than the static couple imbalance output from the spin-balance machine.

4. Effect of Mass Imbalance on Projectile Motion

Mass imbalance on a spinning projectile produces linear deviations of the projectile trajectory off the nominal line of flight. Linear deviations of this type are also referred to as "jump" and can result from a number of sources. Static and couple imbalance are two sources that contribute to the overall jump of the projectile. The deviation of the projectile trajectory due to static imbalance is known as "lateral throw-off". Pure dynamic imbalance causes the projectile to rotate about its principal axis rather than the geometric axis. This rotation causes an additional component of yaw that effects the swerving motion of the projectile. In general, the yawing motion of the projectile can produce a linear deviation in the swerving motion known as aerodynamic jump. The yawing motion due to pure dynamic imbalance produces a contribution to the projectile's aerodynamic jump.

McCoy[3] presents derivations for both the lateral throw-off and aerodynamic jump due to mass asymmetry. The net deviation (or jump) due to both effects is additive, although each component can differ in direction. McCoy's ballistic coordinate system is used here. This system orients the x-axis in the downrange direction, the y-axis oriented up, and the z-axis oriented to the right when looking downrange, as shown in Fig. 6. For simplicity, the nominal line of fire is oriented along the x-axis.

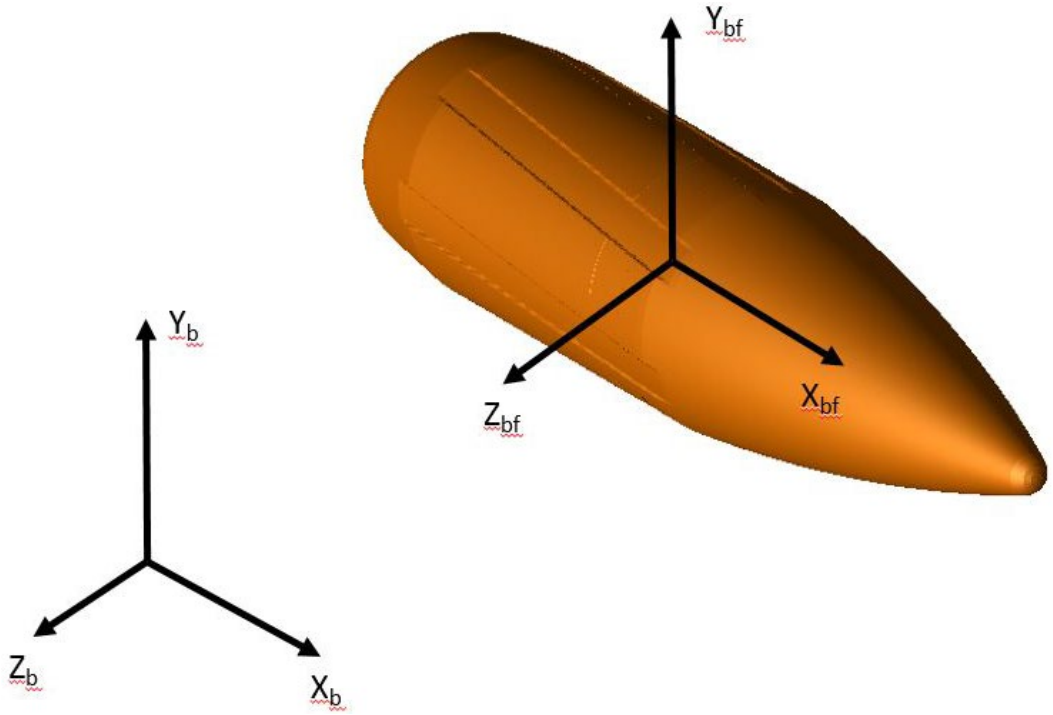

Fig. 6 Ballistic- and body-fixed coordinate systems

There is also a second body-fixed coordinate system in which the physical properties (for example, moments of inertia and mass asymmetries) of the projectile are characterized. Note the x- and z-axes of this coordinate system are oriented in different directions than the coordinate system used in spin-balance measurements shown in Fig. 3. The changes in the orientations have been accounted for in the analysis that follows.

In the following analysis, the most significant difference in the body-fixed and spin-balance coordinate systems is with respect to the circumferential angle measurements in both coordinate systems, as shown in Fig. 7. Effectively, the circumferential angle measurement involves a sign change when going from one coordinate system to another. It is assumed that the circumferential angles from spin-balance measurements are used as the actual measured values, and the required sign change is incorporated in the equations in Section 4.1.

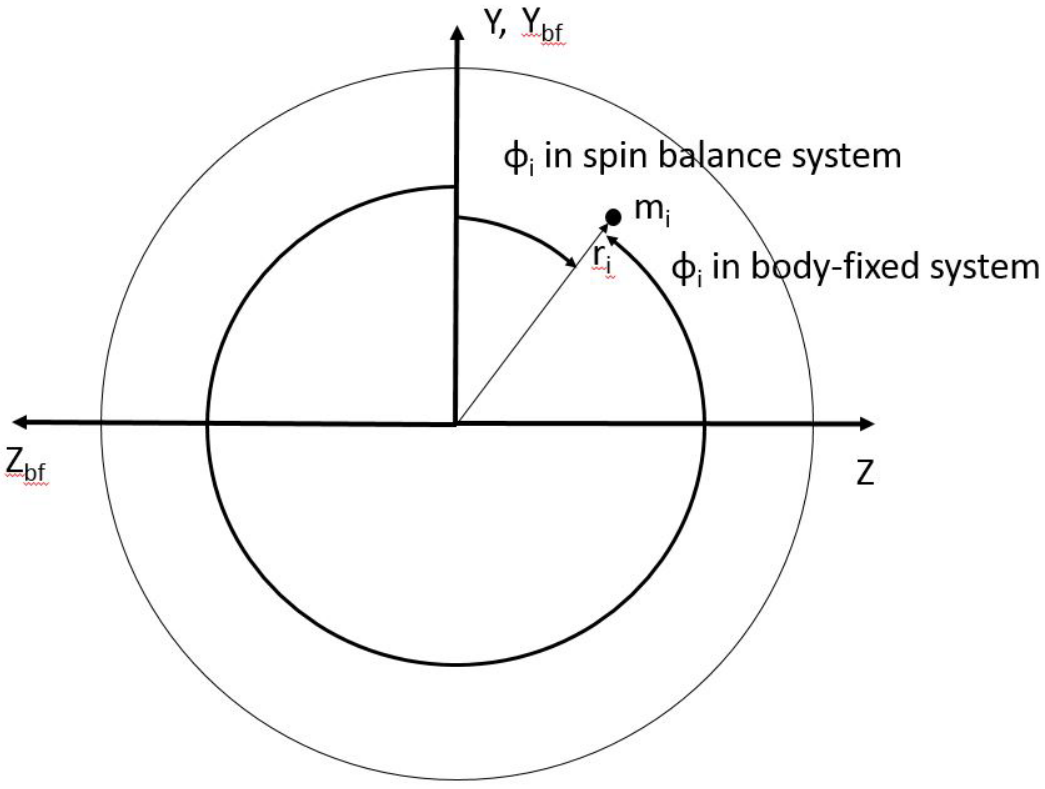

Fig. 7 Circumferential angles in body-fixed and spin-balance coordinate systems (view from nose)

4.1 Lateral Throw-off Due to Static Imbalance

The static imbalance produces an initial deflection of the projectile trajectory off the nominal line of flight, known as throw-off, that increases linearly with range. The deflection will be at 90° to the orientation of the static imbalance as the

projectile leaves the gun tube. For right-hand gun-tube twist, if the offset in the center of gravity produced by the static imbalance is oriented upward in the vertical plane, and the deflection due to throw-off will be to the right when looking downrange. The deflection can be computed as shown in Eq. 52. Here, n is the twist of the rifling (calibers/turn: the number of body diameters traveled in one complete revolution of the projectile [positive for right-hand twist]), ϵ is the magnitude of the lateral displacement of the center of gravity, D is the projectile diameter, and Φ_{S_0} is the circumferential orientation of the center of gravity at muzzle exit relative to the ballistic coordinate frame. The throw-off produces a vertical velocity V_{Y_0} (positive upward) and/or a lateral velocity V_{Z_0} (positive to the gunner's right) at the muzzle that results in an angular deflection off the nominal trajectory when scaled by the forward velocity V_{X_0} of the projectile.

$$T_L = \frac{V_{Y_0} + iV_{Z_0}}{V_{X_0}} = i\left[\left(\frac{2\pi}{n}\right)\left(\frac{\epsilon}{D}\right)e^{i\Phi_{S_0}}\right] = \left(\frac{2\pi}{n}\right)\left(\frac{\epsilon}{D}\right)\left(-\sin\Phi_{S_0} + i\cos\Phi_{S_0}\right) \quad (52)$$

The magnitude of the lateral displacement of the center of gravity ϵ is determined from the magnitude of the static imbalance U_S as shown in Eq. 53, where m is the total mass of the projectile.

$$\epsilon = \frac{U_S}{m} \quad (53)$$

As discussed previously, the throw-off is a function of the angular orientation of the static imbalance when the projectile exits the muzzle, as presented in Eq. 52. In certain specialized applications, it may be possible to determine (or select) the orientation of the static imbalance when the cartridge is placed in the chamber prior to firing. In this case, it is possible to relate the orientation of the static imbalance when the cartridge is inserted to the orientation of the static imbalance as the projectile exits the muzzle, as shown in Eq. 54. The first term in Eq. 54 $(-\emptyset_S)$ accounts for the correction orientation of the static imbalance in the ballistic coordinate frame using the orientation of the static imbalance $\emptyset_S$ as measured in the spin-balance fixture coordinate frame. The second term accounts for the initial orientation of the projectile when inserted in the chamber relative to its position in the spin-balance fixture $\emptyset_{chamber}$ as well as its rotation as the projectile travels down the barrel of length L_{Barrel}. The net sum of these terms provides the orientation of the static imbalance when the bullet reaches the weapon muzzle. In some instances, such as when the contribution of static imbalance to the dispersion of a group of bullets is required to be determined, the initial orientation of the

projectile is a random event and the throw-off can be computed from the first term alone:

$$\Phi_{S_0} = (-\emptyset_S) + (\emptyset_{chamber} + 2\pi n \frac{L_{Barrel}}{D}) \tag{54}$$

4.2 Aerodynamic Jump Due to a Couple (Pure Dynamic) Imbalance

In addition to the lateral throw-off produced by the static imbalance, a projectile that has a dynamic imbalance will have an additional deflection of the trajectory due to aerodynamic jump. The dynamic imbalance will cause the projectile to spin about its principal axis rather than its geometric axis, producing a yaw component in addition to the classical symmetric-projectile epicyclic yawing motion. This additional component of yaw results in a tricyclic yawing motion. As a result, an additional aerodynamic jump component of the swerving motion will also be produced. McCoy[3] provided a derivation of the aerodynamic jump of a projectile with a mass asymmetry, as shown in Eq. 55. Similar to the lateral throw-off, the aerodynamic jump produces a vertical velocity V_{Y_0} (positive upward) and/or a lateral velocity V_{Z_0} (positive to the gunner's right) at the muzzle that results in an angular deflection off the nominal trajectory when scaled by the forward velocity V_{X_0} of the projectile:

$$J_A = \frac{V_{Y_0} + iV_{Z_0}}{V_{X_0}} = k_t^2 \left(\frac{C_{L_\alpha}}{C_{M_\alpha}}\right) \left[(iP\xi_0 - \xi_0') + i\left(\frac{2\pi}{n}\right) K_T e^{i\phi_0}\right] \tag{55}$$

Here C_{L_α} and C_{M_α} are the aerodynamic lift coefficient and pitching moment coefficient slopes respectively, ξ_0 and ξ_0' are the complex yaw and yawing rate at the muzzle and k_t and P are defined by Eqs. 56 and 57:

$$k_t^2 = \frac{I_t}{mD^2} \tag{56}$$

$$P = \frac{I_x}{I_t}\left(\frac{pD}{V}\right) \tag{57}$$

I_x and I_t are the axial and transverse moments of inertia, $\left(\frac{pD}{V}\right)$ is the nondimensional spin rate of the projectile, D is the projectile reference diameter, m is the projectile mass, p is the projectile spin rate, and V is the magnitude of the projectile velocity.

The aerodynamic jump shown in Eq. 55 includes the classical aerodynamic jump for a symmetric projectile as well as the additional term (shown as the last term)

that accounts for the jump due to the mass asymmetry. Here, n is the twist of the rifling (calibers/turn: the number of body diameters traveled for one complete revolution of the projectile [positive for right-hand twist]), K_T is amplitude of the yawing motion produced by the couple imbalance, and ϕ_0 is the orientation of the yaw arm produced by the asymmetry at muzzle exit relative to the vertical coordinate, with positive angles determined from the right-hand rule in the ballistic coordinate frame.

Due to the imbalance, the projectile will rotate about its longitudinal principal axis, producing an additional component to the yawing motion. The amplitude of this additional component of yawing motion can be determined from the principal axis tilt produced by the couple imbalance, as shown in Eq. 58. (Additional details can be found in the Appendix.) Here, U_C is the magnitude of the couple imbalance. Representation of the principal axis tilt in terms of the couple imbalance represents a generalization of the derivation by McCoy[3] for the dynamic imbalance produced by a single small mass removal:

$$K_T = \frac{U_C}{I_t - I_x} \tag{58}$$

The aerodynamic jump due to the couple imbalance U_C is shown in Eq. 59:

$$\begin{aligned} J_A = \frac{V_{Y_0} + iV_{Z_0}}{V_{X_0}} &= ik_t^2 \left(\frac{C_{L_\alpha}}{C_{M_\alpha}}\right)\left(\frac{2\pi}{n}\right)\frac{U_C}{I_t - I_x} e^{i\phi_0} \\ &= k_t^2 \left(\frac{C_{L_\alpha}}{C_{M_\alpha}}\right)\left(\frac{2\pi}{n}\right)\frac{U_C}{I_t - I_x}(-\sin\phi_0 + i\cos\phi_0) \end{aligned} \tag{59}$$

Similar to the lateral throw-off, the aerodynamic jump is a function of the angular orientation of the couple imbalance when the projectile exits the muzzle, as presented in Eq. 60. The first term in Eq. 60 $(-\emptyset_C)$ accounts for the correct vector orientation of the couple imbalance relative the ballistic coordinate frame using the orientation of the couple imbalance $\emptyset_C$ as measured in the spin-balance fixture coordinate frame. The second term accounts for the initial orientation of the projectile when inserted in the chamber relative to its position in the spin-balance fixture $\emptyset_{chamber}$ as well as the rotation of the projectile as it travels down the barrel length L_{Barrel}. If the contribution of dynamic imbalance to the dispersion of a group of bullets is required to be determined, the initial orientation of the projectile is a random event and the aerodynamic jump can be computed from the first term alone.

$$\phi_0 = (-\emptyset_C + \pi/2) + (\emptyset_{chamber} + 2\pi n \tfrac{L_{Barrel}}{D}) \tag{60}$$

While the orientation of the projectile in the weapon chamber can often be considered a random variable, mass imbalance generally produces both a static and

dynamic imbalance, and the amplitude and phases angles associated with both types of mass imbalance are directly related and should not be treated as independent random variables relative to each other.

As shown by McCoy[3], a good approximation to Eq. 59 that simplifies the calculation of the aerodynamic jump can be made by recognizing that the axial moment of inertia is typically much smaller than the transverse moment of inertia. This allows the aerodynamic jump to be computed without specifying the axial or transverse moments of inertia:

$$J_A = \frac{V_{Y_0} + iV_{Z_0}}{V_{X_0}} = i\left(\frac{C_{L_\alpha}}{C_{M_\alpha}}\right)\left[\left(\frac{2\pi}{n}\right)\left(\frac{U_C}{mD^2}\right)e^{i\phi_0}\right] = \left(\frac{C_{L_\alpha}}{C_{M_\alpha}}\right)\left(\frac{2\pi}{n}\right)\left(\frac{U_C}{mD^2}\right)(-\sin\phi_0 + i\cos\phi_0) \tag{61}$$

5. Comparison of Current Analysis with Existing Test Case

McCoy[3] presented theoretical predictions of the lateral throw-off and aerodynamic jump for a 20-mm projectile with a mass imbalance, shown in Fig. 8. The mass imbalance was created by drilling a hole in the base of the projectile at a radius and depth shown in Fig. 8. The resulting material removed weighed 3.18 g. McCoy's theoretical predictions were also compared with experimental measurements for the same projectile, which agreed well. This case is used here to validate aspects of the analysis presented in Sections 3 and 4. In addition to the baseline case presented by McCoy, which positioned the mass offset downward, three additional orientations of the mass imbalance at 90° increments are also considered here.

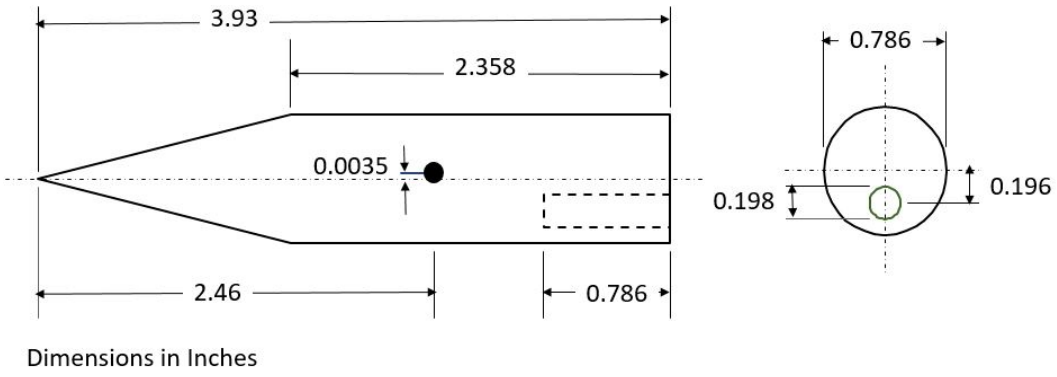

Fig. 8 20-mm projectile with mass offset

To validate the methodology shown in Sections 3 and 4, theoretical predictions of the imbalance at two hypothetical corrections planes were obtained. These results

are shown in Table 2. Conforming to the spin-balance coordinate system with the nose oriented to the left, the left correction planes were located at the cone cylinder junction, and the right correction plane was located at the center of gravity of the mass imbalance. The computed imbalance of the part is shown in the upper half of Table 2 as obtained from appropriate application of Eqs. 16, 17, and 20–25.

Table 2 Hypothetical (theoretical) imbalance and spin-balance correction

Circumferential location of mass offset, φ_i (deg)	**Mass imbalance at left correction plane U_{lc} (mg–cm)**	**Mass imbalance phase angle at left correction plane $\emptyset_{lc}$ (deg)**	**Mass imbalance at right correction plane U_{rc} (mg-cm)**	**Mass imbalance phase angle at right correction plane $\emptyset_{rc}$ (deg)**
180° (down)	0	0	1583	0
270° (gunner's right)	0	0	1583	90
0° (up)	0	0	1583	180
90° (gunner's left)	0	0	1583	–90
Circumferential location of mass offset, φ_i (deg)	Mass correction (addition) at left correction plane (mg)	Mass correction phase angle at left correction plane (deg)	Mass correction (addition) at right correction plane (mg)	Mass correction phase angle at right correction plane (deg)
180° (down)	0	0	1586	180
270° (gunner's right)	0	0	1586	270
0° (up)	0	0	1586	0
90° (gunner's left)	0	0	1586	90

The spin-balance machine typically characterizes the imbalance by the mass required to balance the part and requires that the radius (or diameter) of the part at both correction planes to be specified. For this example, the correction was assumed to be performed at the outer diameter of the cylindrical portion of the projectile although there is no requirement for both radii to be identical. For this example, the spin-balance machine was assumed to be in mass addition mode. The lower portion of Table 2 shows the mass correction required to balance the part as well as the circumferential angle where the correction is to be applied. Note this is the theoretical output of the spin-balance machine when the spin-balance machine is in mass addition mode. The output of the spin-balance machine shows that a correction of 1586 mg is required at the right correction plane to offset the imbalance from the drilled hole in the projectile. (Note the projectile diameter is not exactly 20 mm.) The mass correction is easily obtained from the imbalance U_{lc} and U_{rc}, shown in the upper part of Table 2. The mass of the imbalance correction is less than the mass of the actual mass removal because the correction is made at the outer radius of the projectile rather than at the interior radius where the actual mass removal occurred. No mass imbalance correction is required at the left

correction plane because the center of gravity of the imbalance is centered over the right correction plane.

The analysis described in Section 3 allows the imbalance of the part to be determined. However, the spin-balance machine outputs the correction required to balance the part rather than the actual imbalance. If the spin-balance machine is in mass addition mode, the imbalance located at 180° (π radians) from the circumferential location where the mass correction (addition) is to be applied.

Once the correction plane imbalance magnitudes and phase angles are obtained from the spin-balance mass correction and phase angles, the static and couple imbalance can be computed using Eqs. 46, 47, 50, and 51. The results are shown in Table 3.

Table 3 Static and couple imbalances for 20-mm projectile

Circumferential location of mass offset, φ_i (deg)	Static imbalance U_s (mg-cm)	Static imbalance phase angle $\emptyset_S$ (deg)	Couple imbalance U_c (mg– m^2)	Couple imbalance phase angle $\emptyset_C$ (deg)
180° (down)	1583	0	4331	90
270° (gunner's right)	1583	90	4331	180
0° (up)	1583	180	4331	–90
90° (gunner's left)	1583	270	4331	0

Using the static and couple imbalance, the lateral throw-off and aerodynamic jump were computed, as shown in Table 4. The results are virtually identical to McCoy's results. The results also show the relative differences between the more accurate computation of aerodynamic jump (Eq. 59) and the simplified computation (Eq. 61). The difference in the two approach is about 10% for this example.

Table 4 Lateral throw-off and aerodynamics jump for 20-mm projectile

Circumferential location of mass offset, φ_i (deg)	Lateral throw-off (mil)	Lateral throw-off direction relative to ballistic coordinates	Aerodynamic jump (mil)	Aero jump direction relative to ballistic coordinates	Aerodynamic jump (mil) – simplified computation, Eq. 61
180° (down)	1.12	Right	1.25	Right	1.14
270° (gunner's right)	1.12	Up	1.25	Up	1.14
0° (up)	1.12	Left	1.25	Left	1.14
90° (gunner's left)	1.12	Down	1.25	Down	1.14

6. Results from Imbalance Measurements of Calibration Pins

Calibration pins were constructed to verify the calibration and accuracy of the spin-balance machine. Because of the simple geometry of the part, theoretical calculations of the imbalance were also obtained and compared with the spin-balance measurements. Each of the pins were cylindrical in shape with mass imbalances drilled into the pins at fixed locations. Figure 9 shows a drawing of one of the pins (Pin C). The same hole dimensions were used of each of the pins. With the exception of Pin B, which had a hole drilled at the center, the remaining pins had holes drilled at the same outboard locations.

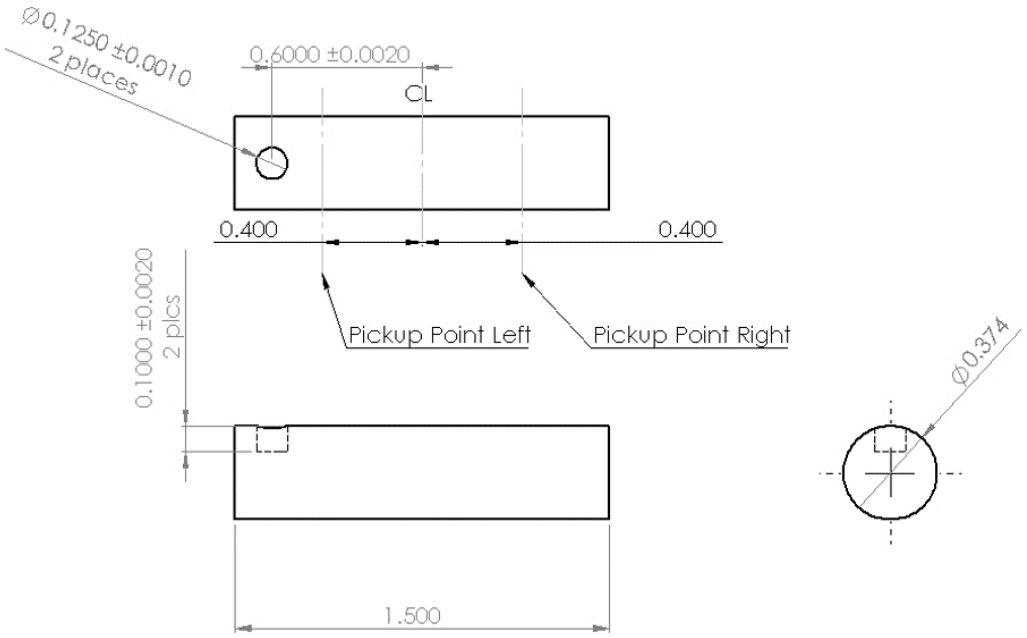

Fig. 9 Schematic of calibration Pin C (dimensions in inches)

Figure 10 shows a drawing of each of the four calibration pins used in the study. Pins A and C had asymmetries drilled at the outboard end of the pins. These pins produced both static and dynamic imbalances. (Pin A had two additional holes drilled that opposed each other and did not contribute to the imbalance.) Pin B had a hole drilled in the middle of the pin, yielding only a static imbalance. Pin D had two holes drilled at opposing ends of the pin and opposite circumference angles, producing a pure couple imbalance with no static imbalance.

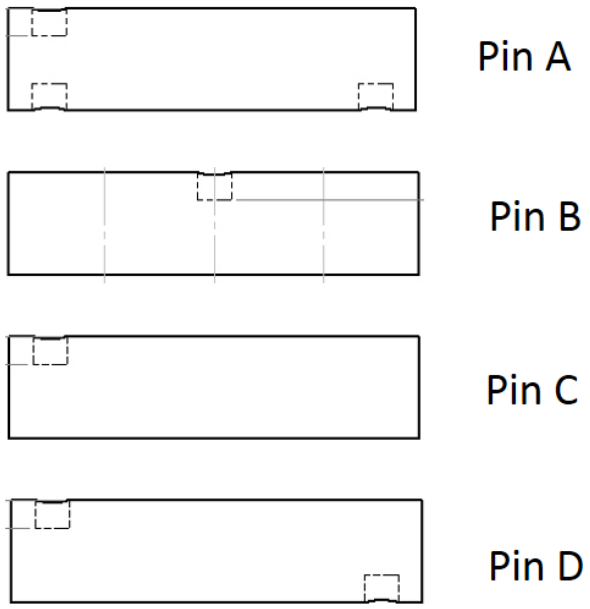

Fig. 10 Calibration pins

Each of the pins were weighed before and after the holes were drilled. This allowed the actual weight of the asymmetry to be measured. The weight measurement of the cylindrical pins before being drilled also allowed the density of the material to be computed. The drilled holes were not perfectly cylindrical because of the curved top produced by the cylindrical shape of the pin itself. The actual volume of the drilled hole was computed numerically and found to be about 5% less than a right cylinder 0.1 inch long. Theoretical predictions of the mass of the hole were based on the measured density and the nominal dimensions from the drawing. The measured mass of the asymmetry was on average 4% higher than the theoretical value. This was assumed to be due to machining tolerances. To account for the mass difference, the hole depth in the theoretical calculations was increased, as shown in Table 5. The increased depth of the hole decreased the theoretical location of the center of gravity of the mass asymmetry by less than 2% of the nominal location. This allowed the theoretical mass of the asymmetry to be equal to the measured mass.

Table 5 Physical properties of mass asymmetry for the four calibration pins

Pin	Measured weight of asymmetry (mg)	Hole depth (cm/inches)	Asymmetry CG from pin centerline (cm)
Nominal	161.5 (theoretical)	0.254 / 0.1	0.341
A	170	0.2667 / 0.105	0.335
B	168	0.2637 / 0.1038	0.3365
C	167	0.2621 / 0.1032	0.3373
D	166.5	0.2616 / 0.103	0.3376

Table 6 presents the measured and theoretical mass corrections at the left and right correction planes. The correction was assumed to be made at the outer diameter of the pins. Note that the location of the correction planes was placed at same location as the pickup locations, so the mass correction would be proportional to the amplitude of the fluctuating part of the pickup forces. The theoretical imbalance at the left and right correction plane was out of phase with each other by 180° except for Pin B, where the imbalances at the left and right correction plane were in-phase. The measured and theoretical phase angle difference between the left and right correction plane differed by less than a few degrees. The measured values of the imbalance for Pin B at both correction planes shows a deviation from the expected symmetry that should exist for this configuration.

Table 6 Measured and theoretical mass corrections at left and right correction planes for the four pins

Pin	Measured left mass correction (mg)	Theoretical left mass correction (mg)	Measured right mass correction (mg)	Theoretical right mass correction (mg)
A	6.5	30.0	149.0	149.9
A	6.6	30.0	148.0	149.9
B	72.9	59.5	59.2	59.5
B	73.0	59.5	59.4	59.5
C	153.2	148.2	8.5	29.6
C	155.7	148.2	8.4	29.6
D	155.8	177.5	156.9	177.5
D	156.7	177.5	156.1	177.5
Average before drilling holes	0.8	0	1.0	0

Pins A and C essentially had the same mass asymmetries, but the asymmetries were located at the opposite ends of the pins. Both pins should show the same measured imbalance when swapped end-for-end or when compared with each other in the same orientation. Table 7 presents the measured and theoretical mass imbalances at the left and right correction planes for Pins A and C with the asymmetries in their nominal location (right and left, respectively, for Pin A and Pin C) and with the asymmetries reversed (left and right, respectively for Pin A and Pin C). Overall, the measured mass imbalance yielded similar results for Pin A and C irrespective of the orientation of the pin when it was measured. (Note that Pins A and C are slightly different because of the slight mass differences in the mass of material removed when drilled. These differences are accounted for in the theoretical predictions.) The differences between the measured and theoretical mass imbalances are most apparent when the imbalance is small.

Table 7 Measured and theoretical mass corrections at left and right correction planes

Pin	Measured left mass correction (mg)	Theoretical left mass correction (mg)	Measured right mass correction (mg)	Theoretical right mass correction (mg)
A (Nominal)	13.9	30.0	144.5	149.9
A (Nominal)	13.5	30.0	145.2	149.9
A (Reversed)	152.0	149.9	16.2	30.0
A (Reversed)	152.4	149.9	15.8	30.0
C (Nominal)	151.0	148.2	17.2	29.6
C (Nominal)	151.1	148.2	16.1	29.6
C (Reversed)	10.6	29.6	143.9	148.2
C (Reversed)	10.5	29.6	143.8	148.2

The measured and theoretical mass corrections/imbalances can be used to determine the resulting static and couple imbalance, as shown in Table 8. The measured static imbalance appears to be about 18% greater than the theoretical value. The measured couple imbalance is about 9% smaller than the corresponding theoretical couple imbalance.

Table 8 Measured and theoretical static and couple imbalances for the four calibration pins

Pin	Measured static imbalance (mg–cm)	Theoretical static imbalance (mg–cm)	Measured couple imbalance (mg–cm^2)	Theoretical couple imbalance (mg–cm^2)
A	67.68	56.95	75.05	86.79
A	67.17	56.95	74.60	86.79
B	62.71	56.53	6.64	0.00
B	62.88	56.53	6.60	0.00
C	68.77	56.33	77.99	85.85
C	70.01	56.33	79.15	85.85
D	1.40	0.00	150.90	171.33
D	1.33	0.00	150.95	171.33
Average before drilling holes	0.74	0	0.4	0

Similar results were found for Pins A and C when the pins were swapped end-for-end, as shown in Table 9. This set of test results were obtained on a different occasion than the results in Table 8. The measured results between pins occasion differences in the results are seen when the Table 9 results are compared with the results in Table 8.

Table 9 Comparison of measured and theoretical values of static and couple imbalance

Pin	Measured static imbalance (mg–cm)	Theoretical static imbalance (mg–cm)	Measured couple imbalance (mg–cm^2)	Theoretical couple imbalance (mg–cm^2)
A (Nominal)	62.13	56.95	76.36	86.79
A (Nominal)	62.68	56.95	76.48	86.79
A (Reversed)	64.49	56.95	81.18	86.79
A (Reversed)	64.87	56.95	81.18	86.79
C (Nominal)	63.56	56.33	81.17	85.85
C (Nominal)	64.13	56.33	80.68	85.85
C (Reversed)	63.34	56.33	74.53	85.85
C (Reversed)	63.34	56.33	74.44	85.85

Overall, the calibration pins provided some measure of validation of the results obtained with the spin-balance machine's ability to measure the static and couple imbalance, although there is some indication that improvements in the calibration of the pickup sensors may be desired.

7. Conclusion

Spin-balance machines typically measure the applied loads at two locations that support the rotating part. The fluctuating component of the applied loads can be directly related to the net effect of the centrifugal forces produced by the individual mass asymmetries within the part. The analysis presented here shows that a projectile with an arbitrary number of mass imbalances can be represented by two strategically located mass imbalances or by a static imbalance and a couple imbalance. The relationship between each of the three types of imbalance is presented. Representation of the imbalance as mass imbalances at two locations allows for a straightforward means of correcting the imbalance.

The imbalance can be directly related to the deflection of the trajectory of the projectile due to the imbalance. While the spin-balance machine used by ARL typically represents the imbalance by mass imbalance at two correction planes, the trajectory deflection is more easily determined from the static and couple imbalances although the static and couple imbalances are easily determined from the two mass imbalances using the analysis shown here.

Measurements on a set of calibration pins were used to benchmark the measurement capability. The measurements were in reasonable agreement with the theoretical predictions. A previously published test case for the trajectory deflection of a 20-mm projectile due to asymmetric mass was also used for additional validation of the capability of determining the trajectory deflection due to mass asymmetry.

8. References

1. American Hofmann Corporation (AHC). Basic balancing theory and application. Lynchburg (VA): AHC; 2014.
2. American Hofmann Corporation (AHC). PC balancer program version 2.0.xx user guide. Lynchburg (VA): AHC; 2013.
3. McCoy RL. Modern exterior ballistics. Atglen (PA): Schiffer Military History; 1999.

Appendix. Derivation of Aerodynamic Jump from Couple Imbalance

A pure dynamic imbalance will produce a contribution to the yawing motion of the projectile and a deflection to the trajectory due to aerodynamic jump from this induced yawing motion. The dynamic imbalance causes the projectile to spin about its longitudinal principal axis rather than its geometric longitudinal axis, producing an angle of attack and subsequent yawing motion. The combination of yawing motion due to the dynamic imbalance along with the normal epicyclic yawing motion of a symmetric projectile produces what is referred to as a tricyclic yawing motion.

To determine the aerodynamic jump due to the dynamic imbalance, the principle axis tilt relative to the geometric axis must be determined. The moments of inertia in the body-fixed (geometric) axis frame can be represented by the inertia matrix in Eq. A-1. For a symmetric projectile, the diagonal terms consist of the axial moment of inertia ($I_{xx} = I_x$) and the transverse moment of inertia ($I_{yy} = I_{zz} = I_t$) and the off-diagonal terms are zero.

$$\begin{bmatrix} I_{xx} & -I_{xy} & -I_{xz} \\ -I_{xy} & I_{yy} & -I_{yz} \\ -I_{xz} & -I_{yz} & I_{zz} \end{bmatrix} \tag{A-1}$$

The mass asymmetries contributes components to the diagonal and off-diagonal terms in the inertia matrix as shown in Eq. A-2. Here, the location of the individual mass asymmetries (x_i, y_i, z_i) of mass m_i are referenced relative to the body-fixed coordinate system (spin-balance measurement coordinate system) located at the body center of gravity, as shown in Fig. 6 of the main report.

$$
\begin{aligned}
I_{xx} &= I_x^{Symmetric} + \sum_{i=1}^{i=n} m_i\,(y_i^2 + z_i^2) \\
I_{yy} &= I_t^{Symmetric} + \sum_{i=1}^{i=n} m_i\,(x_i^2 + z_i^2) \\
I_{zz} &= I_t^{Symmetric} + \sum_{i=1}^{i=n} m_i\,(x_i^2 + y_i^2) \\
I_{xy} &= \sum_{i=1}^{i=n} m_i\,x_i y_i \\
I_{xz} &= \sum_{i=1}^{i=n} m_i\,x_i z_i \\
I_{yz} &= \sum_{i=1}^{i=n} m_i\,y_i z_i
\end{aligned}
\tag{A-2}
$$

The principal moments of inertia and the principal directions can be obtained from the eigenvalues and eigenvectors associated with the inertia matrix. The primary interest here is the principal direction along the spin axis $\vec{P}_1$, as this will allow the principal axis tilt to be determined. The eigenvalue associated with the spin axis is approximately equal to I_{xx} for small mass asymmetries. Computing the eigenvector associated with this eigenvalue allows the direction of the principal axis to be determined:

$$
\vec{P}_1 = \frac{1}{\sqrt{1 + \left(\frac{I_{xy}}{I_t - I_x}\right)^2 + \left(\frac{I_{xz}}{I_t - I_x}\right)^2}} \left(\tilde{\imath} + \left(\frac{I_{xy}}{I_t - I_x}\right)\tilde{\jmath} + \left(\frac{I_{xz}}{I_t - I_x}\right)\tilde{k}\right) \tag{A-3}
$$

As shown in Eq. A-4, the couple imbalance is related to the combined effect of the individual imbalances as measured in the spin-balance fixture coordinates, as shown in Eqs. 42 and 43 from Section 3.3 of the main report.

$$
\begin{aligned}
U_C \cos \emptyset_C &= -\sum_{i=1}^{i=n} m_i\, r_i (L_i - L_{CG}) \sin \emptyset_i \\
U_C \sin \emptyset_C &= \sum_{i=1}^{i=n} m_i\, r_i (L_i - L_{CG}) \cos \emptyset_i
\end{aligned}
\tag{A-4}
$$

The off-diagonal moment of inertia terms I_{xy} and I_{xz} can be related to the couple imbalance measured on the spin-balance fixture. The location of the asymmetries (x_i, y_i, z_i) in body-fixed ballistic coordinate frame can be transformed to their locations in the spin-balance coordinate frame ($L_i, r_i, \emptyset_i$), as seen in Figs. 6 and 7 of the main report.

$$x_i = -(L_i - L_{CG})$$

$$y_i = r_i \cos(-\emptyset_i) = r_i \cos(\emptyset_i)$$

$$z_i = r_i \sin(-\emptyset_i) = -r_i \sin(\emptyset_i)$$

$$I_{xy} = \sum_{i=1}^{i=n} m_i\, x_i y_i = -\sum_{i=1}^{i=n} m_i\,(L_i - L_{CG}) r_i \cos(\emptyset_i) = -U_C \sin(\emptyset_C) = +U_C \sin(-\emptyset_C) \tag{A-5}$$

$$I_{xz} = \sum_{i=1}^{i=n} m_i\, x_i z_i = +\sum_{i=1}^{i=n} m_i\,(L_i - L_{CG}) r_i \sin(\emptyset_i) = -U_C \cos(\emptyset_C) = -U_C \cos(-\emptyset_C)$$

Considering just the component of the yawing motion due to the dynamic imbalance in the absence of the epicyclic yawing motion, the freestream velocity vector would be aligned with the principal axis associated with the spin axis $\vec{P}_1$.

$$\begin{aligned}\frac{\vec{V}}{|\vec{V}|} &= \frac{V_x}{|\vec{V}|}\tilde{\imath} + \frac{V_y}{|\vec{V}|}\tilde{\jmath} + \frac{V_z}{|\vec{V}|}\tilde{k} = \overrightarrow{-P_1} \\ &= \frac{-1}{\sqrt{1 + \left(\frac{I_{xy}}{I_t - I_x}\right)^2 + \left(\frac{I_{xz}}{I_t - I_x}\right)^2}}\left(\tilde{\imath} + \left(\frac{I_{xy}}{I_t - I_x}\right)\tilde{\jmath}\right. \\ &\left. + \left(\frac{I_{xz}}{I_t - I_x}\right)\tilde{k}\right) \\ &= \frac{-1}{\sqrt{1 + \left(\frac{I_{xy}}{I_t - I_x}\right)^2 + \left(\frac{I_{xz}}{I_t - I_x}\right)^2}}\left(\tilde{\imath} + \left(\frac{U_C \sin(-\emptyset_C)}{I_t - I_x}\right)\tilde{\jmath}\right. \\ &\left. + \left(\frac{-U_C \cos(-\emptyset_C)}{I_t - I_x}\right)\tilde{k}\right)\end{aligned} \tag{A-6}$$

For small asymmetries, the resulting angle of attack components are small and the complex yaw can be written as shown in Eq. A-7.

$$\begin{aligned}\xi_T &= \frac{V_Y + iV_z}{|\vec{V}|} = \alpha_T + i\beta_T = K_T e^{i\phi_T} \\ &= \left(\frac{-U_C}{I_t - I_x}\right)(\sin(-\emptyset_C) - i\cos(-\emptyset_C))\end{aligned} \tag{A-7}$$

From Eq. A-7, the magnitude of the yaw K_T due to the couple imbalance is obtained and shown in Eq. A-8, and the relation between the orientation of the yaw arm in the ballistic frame to the orientation of the vector orientation of the couple in the spin-balance frame resulting from the dynamic imbalance is shown in Eq. A-9.

$$K_T = \left(\frac{U_C}{I_t - I_x}\right) \tag{A-8}$$

$$\emptyset_C = \phi_0 - \pi/2 \tag{A-9}$$

McCoy[1] provided a derivation of the aerodynamic jump of a projectile with a mass asymmetry, as shown in Eq. A-10. Similar to the lateral throw-off, the aerodynamic jump produces a vertical velocity V_{Y_0} (positive upward) and/or a lateral velocity V_{Z_0} (positive to the gunner's right) at the muzzle that results in an angular deflection off the nominal trajectory when scaled by the forward velocity V_{X_0} of the projectile. The aerodynamic jump includes the classical aerodynamic jump for a symmetric projectile as well as the additional term (shown as the last term of Eq. A-10), which accounts for the jump due to the mass asymmetry:

$$J_A = \frac{V_{Y_0} + iV_{Z_0}}{V_{X_0}} = \; k_t^2 \left(\frac{C_{L_\alpha}}{C_{M_\alpha}}\right)\left[(iP\xi_0 - \xi_0') + i\left(\frac{2\pi}{n}\right)K_T e^{i\phi_0}\right] \tag{A-10}$$

Here C_{L_α} and C_{M_α} are the aerodynamic lift coefficient and pitching moment coefficient slopes respectively, ξ_0 and ξ_0' are the complex yaw and yawing rate at the muzzle and k_t and P are defined in Eqs. A-11 and A-12.

$$k_t^2 = \frac{I_t}{mD^2} \tag{A-11}$$

$$P = \frac{I_x}{I_t}\left(\frac{pD}{V}\right) \tag{A-12}$$

I_x and I_t are the axial and transverse moments of inertia, $\left(\frac{pD}{V}\right)$ is the nondimensional spin rate of the projectile, D is the projectile reference diameter, m is the projectile mass, p is the projectile spin rate, and V is the magnitude of the projectile velocity.

The last term in Eq. A-10 represents the aerodynamic jump contribution due to the mass asymmetry. Here, n is the twist of the rifling (calibers/turn: the number of body diameters traveled for one complete revolution of the projectile [positive for right-hand twist]), K_T is amplitude of the yawing motion produced by the couple imbalance, and ϕ_0 is the orientation of the yaw arm produced by the asymmetry at

[1] McCoy RL. Modern exterior ballistics. Atglen (PA): Schiffer Military History; 1999.

muzzle exit relative to the vertical coordinate with positive angles determined from the right-hand rule in the ballistic coordinate frame.

Substituting Eqs. A-8 and A-9 into the last term of Eq. A-10, the aerodynamic jump due to the mass asymmetry is obtained, as shown in Eq. A-13. Here the aerodynamics jump is related to the magnitude and angular orientation of the couple imbalance U_C and $\emptyset_C$, respectively, as measured from the spin-balancing procedure.

$$\begin{aligned} J_A = \frac{V_{Y_0} + iV_{Z_0}}{V_{X_0}} &= ik_t^2 \left(\frac{C_{L_\alpha}}{C_{M_\alpha}}\right)\left(\frac{2\pi}{n}\right)\frac{U_C}{I_t - I_x} e^{i\phi_0} \\ &= k_t^2 \left(\frac{C_{L_\alpha}}{C_{M_\alpha}}\right)\left(\frac{2\pi}{n}\right)\frac{U_C}{I_t - I_x}(-\sin\phi_0 + i\cos\phi_0) \end{aligned} \tag{A-13}$$

McCoy[1] presented a derivation of the aerodynamic jump for the dynamic imbalance produced by a single small mass removal. Eq. A-13 represents the aerodynamic jump due to an arbitrary distribution of multiple mass asymmetries in terms of the couple produced by the asymmetries and represents a generalization of the result presented by McCoy.

[1] McCoy RL. Modern exterior ballistics. Atglen (PA): Schiffer Military History; 1999.

1 (PDF)	DEFENSE TECHNICAL INFORMATION CTR DTIC OCA
1 (PDF)	CCDC ARL FCDD RLD CL TECH LIB
4 (PDF)	CCDC ARL FCDD RLW LE P WEINACHT T PUCKETT G OBERLIN FCDD RLW LH J GARNER